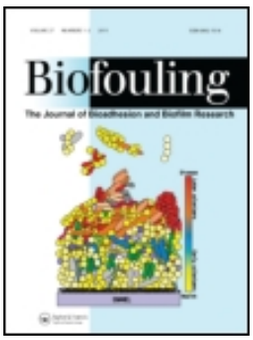

Biofouling

ISSN: 0892-7014 (Print) 1029-2454 (Online) Journal homepage: http://www.tandfonline.com/loi/gbif20

Corrosion of mild steel underneath aerobic biofilms containing sulfate-reducing bacteria part I: At low dissolved oxygen concentration

Whonchee Lee , Zbigniew Lewandowski , Sathoshi Okabe , William G Characklis & Recep Avcl

To cite this article: Whonchee Lee , Zbigniew Lewandowski , Sathoshi Okabe , William G Characklis & Recep Avcl (1993) Corrosion of mild steel underneath aerobic biofilms containing sulfate-reducing bacteria part I: At low dissolved oxygen concentration, Biofouling, 7:3, 197-216, DOI: 10.1080/08927019309386254

To link to this article: https://doi.org/10.1080/08927019309386254

Published online: 09 Jan 2009.

Biofouling, 1993, Vol. 7, pp. 197–216
Reprints available directly from the publisher
Photocopy permitted by license only

CORROSION OF MILD STEEL UNDERNEATH AEROBIC BIOFILMS CONTAINING SULFATE-REDUCING BACTERIA PART I: AT LOW DISSOLVED OXYGEN CONCENTRATION

WHONCHEE LEE*, ZBIGNIEW LEWANDOWSKI*, SATHOSHI OKABE*, WILLIAM G CHARACKLIS* and RECEP AVCI**

*Center for Interfacial Microbial Process Engineering, Montana State University, Bozeman, MT 59717, USA; **Physics Department, Montana State University, Bozeman, MT 59717, USA*

(Received 1 September 1992; in final form 20 March 1993)

The sulfate-reducing bacteria (SRB)-enhanced corrosion of mild steel in the presence of 1.5 $mg \cdot l^{-1}$ dissolved oxygen (DO) in bulk liquid was investigated. The biofilm process analysis was combined with microelectrode measurements, electrochemical measurements, and surface analysis. In the early stages of biofilm accumulation, the cathodic polarization and the decreasing corrosion rate were attributed to DO consumption by aerobic bacteria. During that time, limited SRB activity was observed. The DO concentration near the steel surface was between 0.6 and 1 $mg \cdot l^{-1}$. After total depletion of dissolved oxygen near the steel surface, the cathodic depolarization and the increased corrosion rate were associated with the proliferation of SRB near the steel surface. Auger electron spectroscopy analysis indicated localized sulfide attack. High pit density appeared where the coincidence of oxygen and sulfur occurred. The bottom of the pit was enriched with sulfur.

KEYWORDS: biofilm, sulfate-reducing bacteria, corrosion, microelectrode

INTRODUCTION

Microbial corrosion results from the presence of biofilm at the metal surface. The biofilm system consists of three compartments: (1) bulk liquid, (2) biofilm, and (3) substratum. Biofilms influence corrosion processes by changing the local chemistry near the metal surface. Interfacial water chemistry between the metal surface and the biofilm is determined by: (1) corrosion processes; (2) microbial activity and the presence of metabolic products; (3) mass transport processes within the system compartments; and (4) bulk water chemistry. Both corrosion and biofilm accumulation are dynamic processes. Consequently, the interfacial water chemistry changes with time. Microbial corrosion is the net result of the interaction between various compartments which are in dynamic flux. To study microbial corrosion, both the conceptual models and experimental methodology must reflect and respond to these circumstances.

The goal of this work was to describe in an integrated manner the chemical, microbiological, and physical processes in a biofilm system that contribute to microbial corrosion. A biofilm system containing SRB on a mild steel substratum under aerobic bulk liquid was chosen, because it is frequently encountered in industrial water systems.

In an abiotic and an aerobic system, the corrosion rate of mild steel in seawater is controlled by the cathodic reaction (*e.g.* the reduction of dissolved oxygen), which is under either diffusional or mixed (reaction + diffusion) control, depending on fluid dynamics

and the history of the corroded steel (Bonnel *et al.*, 1983). Corrosion rate decreases with time because oxygen transport rate to the metal surface decreases as a result of accumulation of corrosion products at the metal surface. In a biotic, anaerobic system, SRB may enhance corrosion by generating hydrogen sulfide. It has been hypothesized that protons (King *et al.*, 1973) or hydrogen sulfide (Costello, 1974) might serve as electron acceptors, instead of oxygen, for the cathodic reaction, producing hydrogen:

(a) hydrogen ion reduction at iron sulfide

$$2H^{+} + 2e^{-} = 2H = H_2 \tag{1}$$

(b) hydrogen sulfide reduction:

$$2H_2S + 2e^{-} \rightarrow 2HS^{-} + H_2 \tag{2}$$

SRB subsequently oxidize the molecular hydrogen which prevents polarization of the cathode. HS– ions react with ferrous ions (from anodic dissolution) to produce iron sulfide:

$$Fe^{+2} + HS^{-} \rightarrow FeS + H^{+} \tag{3}$$

Iron sulfide is cathodic to steel and enhances corrosion through cathodic depolarization (Smith *et al.*, 1975). Thus, SRB enhance corrosion of steel through both direct (hydrogen removal) and indirect (hydrogen sulfide and iron sulfide production) processes. Because most SRB-enhanced corrosion is found in the form of localized corrosion, local SRB activity may significantly influence the rate and extent of corrosion. The importance of dissolved oxygen to the SRB-enhanced corrosion of ferrous metals and alloys has been emphasized by several authors (Hardy & Brown, 1984; Starkey, 1985; Hamilton, 1990; Moosavi *et al.*, 1990). Pitting corrosion was the characteristic mode of attack, and deep pits were frequently found. Hamilton and Maxwell (1985) developed a qualitative biofilm model of anaerobic microbial corrosion where biofilm SRB growth required that appropriate physicochemical conditions be created by other facultative and anaerobic organisms within the biofilm. In the present study attempts were made to determine the conditions under which SRB can initiate and/or accelerate localized corrosion of mild steel underneath an aerobic biofilm. SRB were grown under a low DO concentration (1.5 $mg \cdot l^{-1}$ in bulk liquid). The corrosion process was quantified during biofilm accumulation.

MATERIALS AND METHODS

Reactor

The experiment was conducted in a closed flow channel reactor with dimensions 1.00 m × 0.15 m × 0.30 m containing a working volume of 4.5 l and a wet surface area of 0.35 m^2 (Fig. 1). The reactor was made of polycarbonate and had a recirculation loop to provide sufficient mixing. The average flow velocity was approximately 0.3 $m \cdot s^{-1}$. The reactor was initially operated as a batch reactor until biofilm accumulated on the polycarbonate surface. Subsequently, the reactor was operated as a continuous flow reactor at a dilution rate (volumetric flow rate divided by working volume) of 0.45 h^{-1}. Twenty-four corrosion coupons were flush mounted into the bottom of the reactor 12 h after switching to

continuous flow. Temperature was maintained at 30°C. The original bulk DO concentration was set at 1.5 $mg \cdot l^{-1}$ after switching to continuous flow by purging nitrogen through the reactor at a constant flow rate (0.2 $ml \cdot min^{-1}$). After the flow of nitrogen was set, the bulk DO concentration dropped to 0.4 $mg \cdot l^{-1}$ as a result of aerobic microbial activity.

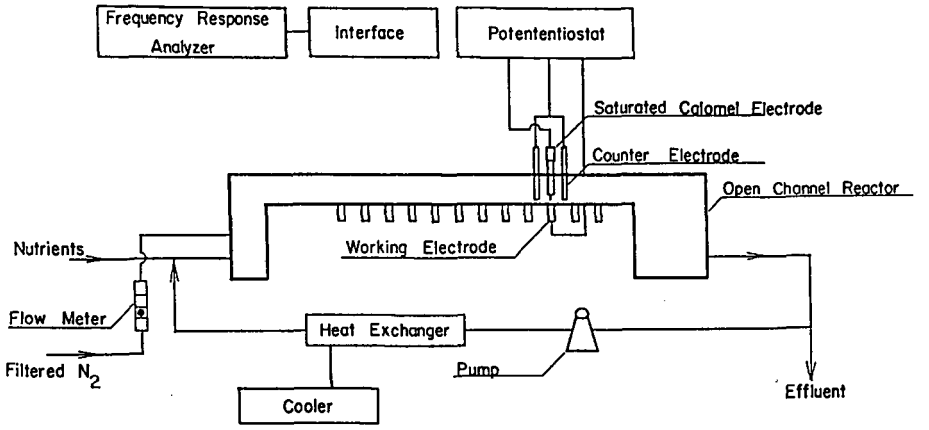

Fig. 1 Closed channel flow reactor with dimensions 1.00 m × 0.15 m × 0.30 m and with a working volume of 4.5 l and a surface area of 0.35 m^2.

Media and Biofilm Growth Conditions

Biofilm was grown in a medium containing 3.5 $g \cdot l^{-1}$ artificial seawater (Instant Ocean, Aquarium Systems, Mentor, OH), 10 $mg \cdot l^{-1}$ glucose, 25 $mg \cdot l^{-1}$ sodium lactate, 25 $mg \cdot l^{-1}$ sodium acetate, 10 $mg \cdot l^{-1}$ yeast extract, 10 $mg \cdot l^{-1}$ NH_4Cl, and 2 $mg \cdot l^{-1}$ Na_2HPO_4. This medium was inoculated with *Pseudomonas aeruginosa, Klebsiella pneumonia, and Desulfovibrio desulfuricans.* The experiment was not conducted aseptically which resulted in an undefined mixed culture biofilm accumulation.

Corrosion Coupons

Disks of AISI 1018 mild steel from Metal Samples Incorporated (Mumford, AL) 15.9 mm in diameter were cast in epoxide resin (Buehler). The coupons were polished with grit papers (120, 200, 320, 400, and 600) followed by ultrasonic cleaning in 100% alcohol for 1 min and dried in air at room temperature. Nominal composition of the mild steel referred to in this paper was 0.20% C, 0.01% P, 0.014% S and 0.76% Mn, with the balance being Fe.

Microelectrode Measurements

Construction of a DO microelectrode and an iridium/iridium oxide pH microelectrode were described previously (Lewandowski *et al.*, 1989; VanHoudt *et al.*, 1992). The sensing tip diameters were typically in the range of 3 to 15 μm. The DO microelectrode was calibrated using the reactor effluent by aeration and subsequent purging with pure nitrogen. The 2 calibration end points were taken in air-saturated and totally deaerated solutions. The microelectrode was polarized cathodically (–0.8 V) against an Ag/AgCl reference electrode, and the current in the circuit was measured with a picoammeter.

The iridium/iridium oxide pH microelectrode was calibrated with standard pH buffer solutions (4 and 10). It exhibited a high Nernstian slope (70 mV/pH against an Ag/AgCl reference electrode). The pH was measured using a high impedance electrometer, 10^{15} ohms.

Microelectrodes were mounted on a micromanipulator (World Precision) and penetrated the biofilm perpendicular to the metal surface. DO concentration and pH were measured in 100 μm intervals.

Corrosion Measurements

A graphite counter electrode was positioned 5 mm above the metal coupon, and a saturated calomel electrode (SCE) was placed next to the metal coupon. Open circuit corrosion potential, cathodic polarization, anodic polarization, and AC impedance were measured on different metal coupons about every week during biofilm accumulation. DC measurements were made using a Princeton Applied Research Corporation (PARC) 273 Potentiostat/Galvanostat interfaced with a computer. AC measurements were made using Solartron 1250 Frequency Response Analyzer through the PARC 273 Potentiostat with a 92 Electrochemical Interface controlled by a computer. Measurements were carried out at the corrosion potential over a frequency range of 1 mHz to 10 KHz (10 points for each decade). The applied ac voltage was 10 mV (rms). Polarization resistance (R_p) from AC measurements was determined using the CIRFIT-computer program (Kending *et al.*, 1983). Solution resistance (R_s) was constant, about 25 ohms, during the entire experiment. The error (R_s/R_p) in the DC measurements was estimated between 0.2% and 1.4%. The relatively small error indicated that polarization curves were not distorted by the solution resistance.

Microbiological Analysis

Bacterial counts in the biofilm were determined by the five tube multiple dilution Most Probable Number (MPN) method (Clesceri *et al.*, 1989). The metal coupons coated with biofilm were removed from the reactor. The biofilm was mechanically removed, transferred to 15 ml of sterile water and homogenized to disperse the sessile bacteria. A dilution series down to 10^{-10} was prepared from 1 ml of dispersed biofilm. MPN counts were converted into surface area densities (numbers of cells·cm^{-2}) by converting the MPN values to total numbers per sample and dividing by the measured substratum surface area. Numbers of bacteria in the bulk liquid were determined using the MPN method. Postgate medium B was used for the enumeration of SRB, and fluid thioglycollate was used for general anaerobic bacteria. Since Postgate medium B contains sodium lactate, the results from MPN counts indicate only lactate-utilizing SRB. Numbers of heterotrophic bacteria, both in the biofilm and bulk liquid, were determined by Spread Plate Method using R2A agar.

Substrate Removal Rate

The concentrations of dissolved organic carbon, both in the influent and effluent, were determined by filtering 100 ml of solution through a Nuclepore membrane (Nuclepore Corporation, Pleasanton CA, No. 111107; average pore size 0.2 μm). The filtrates were analyzed using a Dohrmann DC-80 Total Organic Carbon Analyzer.

The substrate removal rate was calculated as follows (Characklis, 1990):

$$R_g = DV\frac{(s_i - s)}{A} - \frac{V}{A}\frac{ds}{dt} \tag{4}$$

where

R_g	=	sessile bacteria substrate removal rate	$(ml^{-2}t^{-1})$
D	=	dilution rate of reactor feed	(t^{-1})
s_i	=	influent soluble organic carbon concentration	(ml^{-3})
s	=	effluent soluble organic carbon concentration	(ml^{-3})
A	=	reactor wetted surface area	(l^2)
V	=	reactor volume	(l^3)
t	=	time	(t)

Film Thickness

The corroded coupons with biofilm were removed from the reactor and fixed for 8 h in 2% glutaraldehyde diluted with filter-sterilized artificial seawater. The sample was dehydrated in a graded series of ethanol baths using two changes, 1 h in 70% then 1 h in 95% ethanol, and overnight in 100% ethanol. The biofilm sample and corrosion products were embedded in polymer using the method described by Emmanual and Hornbeck (1987). The sample was immersed into a solution of 1 part of 100% ethanol and 1 part of washed methyl methacrylate monomer (MMA) (4% sodium hydroxide + 96% methyl methacrylate monomer) at room temperature overnight to remove the water. Two changes of washed MMA were performed overnight at 4°C to retard polymerization and to complete the infiltration of monomer. The sample was placed in catalyzed, washed MMA (1.2 to 1.3 g benzoyl peroxide for every 100 ml washed MMA) and infiltrated overnight at 4°C. It was then brought to room temperature and allowed to polymerize slowly. The polymerized block was cross cut perpendicular to the deposit in 2–3 mm thick slices using a diamond wafering blade on a Buehler Isomet low-speed saw. The slices were ground with No. 600 and then 10 μm grit Norton Tufbak Durite sandpapers and polished with 1 μm then 0.3 μm water-based alumina polishing suspension. Average film thickness was measured with a light microscope at 5 different locations.

Surface Analysis

The biofilm and loosely accumulated corrosion products were mechanically removed from the steel coupons. The coupons were rinsed with distilled water, degreased in 100% alcohol, and dried in a desiccator. Auger electron spectroscope (AES) (Physical Electronic, model 595) was used for analysis. The system was equipped with a scanning electron microscope (SEM), a differentially pumped ion gun for sputter etching in ultra-high vacuum (UHV) conditions (about 2×10^{-10} torr), a DEC-PDP 11/04 computer for control and data acquisition, and a fast entry lock for rapid sample introduction into the UHV system. A 5 KeV incident beam, with about 0.2 μm beam diameter and about 0.1 uA beam current, was used for the study. The sputtering rate was about 9 $nm \cdot min^{-1}$. AES analysis included surface morphology, elemental analysis, and elemental mapping.

RESULTS

Substrate Removal and Biofilm Development

The reactor was operated for 5 weeks. The organic carbon removal rate rapidly increased to about 2 $g \cdot m^{-2} \cdot d^{-1}$ by the end of the fifth day then slowly increased to about 2.5 $g \cdot m^{-2} \cdot d^{-1}$ by the end of the fifth week (Fig. 2). The soluble organic carbon in the effluent was about 2 $mg \cdot l^{-1}$ during the last week. The bulk liquid sulfate concentrations

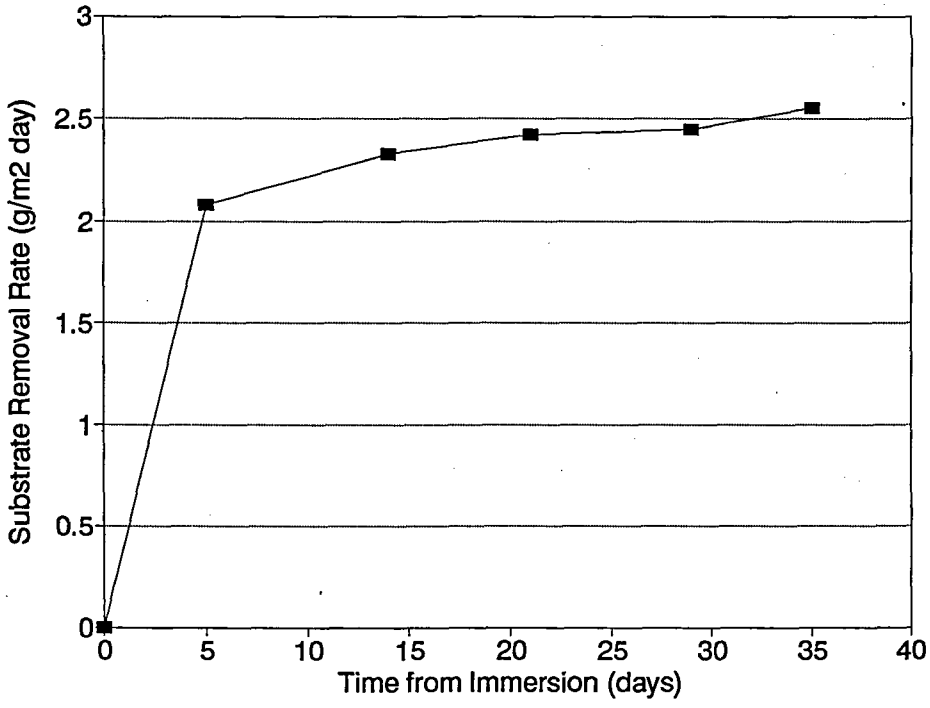

Fig. 2 Substrate removal rate *vs* time.

was about 250 $mg \cdot l^{-1}$. There was no detectable difference in sulfate concentrations between influent and effluent, and no sulfide was detected in the bulk liquid during the entire experiment.

Biofilm accumulation was spatially heterogeneous for the first 2 weeks. For the last 3 weeks, the biofilm uniformly covered the steel surface and the biofilm surface was filamentous. The average film thickness (biofilm + corrosion products) increased from 0.4 mm on the fifth day to 2.7 mm by the end of fifth week (Fig. 3). Surface area density of SRB increased from 3×10^4 cells·cm^{-2} on the fifth day to 4×10^7 cells·cm^{-2} by the end of the second week then increased to 1.5×10^8 cells·cm^{-2} by the end of the fifth week (Fig. 4). Surface area density of heterotrophic bacteria slowly increased from 1×10^8 cells·cm^{-2} on the fifth day, to 1×10^9 cells·cm^{-2} by the end of the second week, and then to 3×10^9 cells·cm^{-2} by the end of the fifth week (Fig. 4). This observation corresponds well with the changes in organic carbon removal rate. MPN counts for SRB at the end of experiment showed that there were more SRB accumulated at and/or near the steel surface (5×10^7 cells·cm^{-2}) than in the uppermost part of biofilm (1×10^2 cells·cm^{-2}) (Fig. 5). The increase in numbers of viable SRB in the bulk liquid during biofilm accumulation (Fig. 6) was a result of detachment of biofilm since SRB cannot grow in an oxygenated environment. The numbers of total sessile cells were about two orders of magnitude higher than the total planktonic cells during the entire experiment (Figs 4 & 6). Substrate removal by planktonic cells was therefore insignificant as compared to that by sessile biofilm cells.

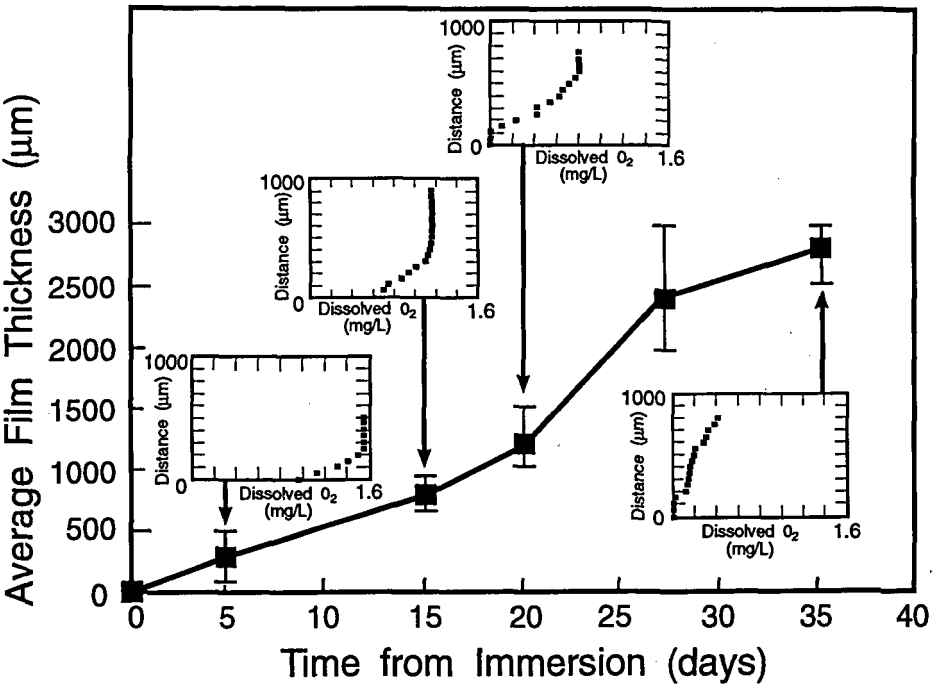

Fig. 3 Progression of film (biofilm + corrosion products) thickness and corresponding DO profiles. Steel surface is indicated at distance = 0 only for the first two DO profiles.

Oxygen and pH Gradients Within the Deposits

DO concentration in the bulk liquid decreased from 1.5 $mg \cdot l^{-1}$ at the beginning of experiment to 0.4 $mg \cdot l^{-1}$ at the end of experiment. Microelectrode measurements indicated that a DO concentration near the steel surface was 1.0 $mg \cdot l^{-1}$ at the end of the first and 0.6 $mg \cdot l^{-1}$ at the end of the second week (Fig. 3). DO concentration near the steel surface reached zero by the end of the third week.

The authors attempted to calculate the oxygen removal rate by determining the flux of oxygen from the DO profiles. However, it was impossible to determine the diffusion layer thickness because of the filamentous nature of the biofilm. The biofilm surface could not have been located precisely. Consequently, it was impossible to accurately determine oxygen consumption rate. However, the decrease in DO concentration in bulk liquid from 1.5 $mg \cdot l^{-1}$ to 0.4 $mg \cdot l^{-1}$ and the increase in surface area density of heterotrophic bacteria in the biofilm from 1×10^8 to 3×10^9 $cells \cdot cm^{-2}$ indicate that oxygen consumption increased as a result of biofilm growth.

The bulk liquid pH was 7. Microelectrode measurements did not indicate any pH gradient through the biofilm to the steel surface for the entire experiment.

Corrosion Rate of Mild Steel During Biofilm Accumulation

During the first 2 weeks of biofilm accumulation, yellowish brown ferric hydrate accumulated on the steel surface. The deposits darkened by the third week and became black by the fourth and fifth weeks.

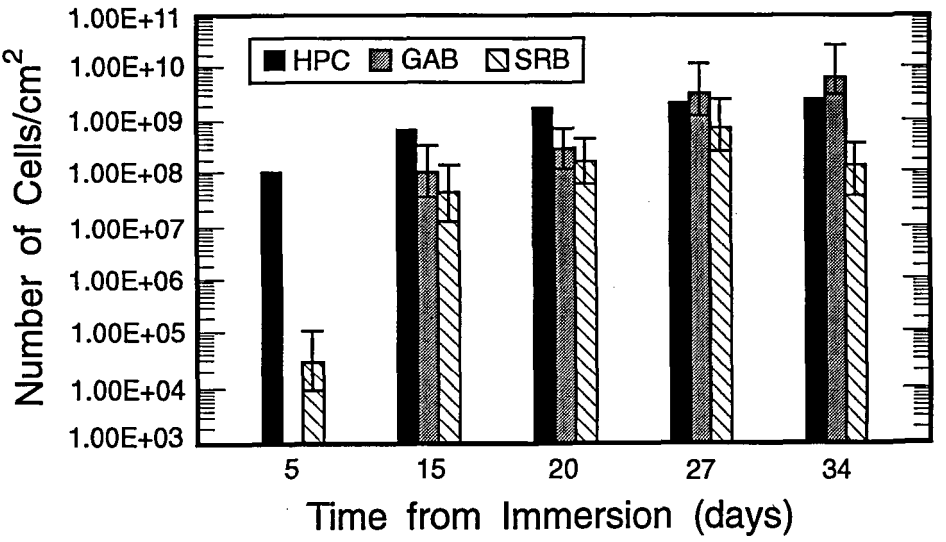

Fig. 4 Microbial accumulation in biofilm at different time periods. The bars indicate 95% confidence limits.

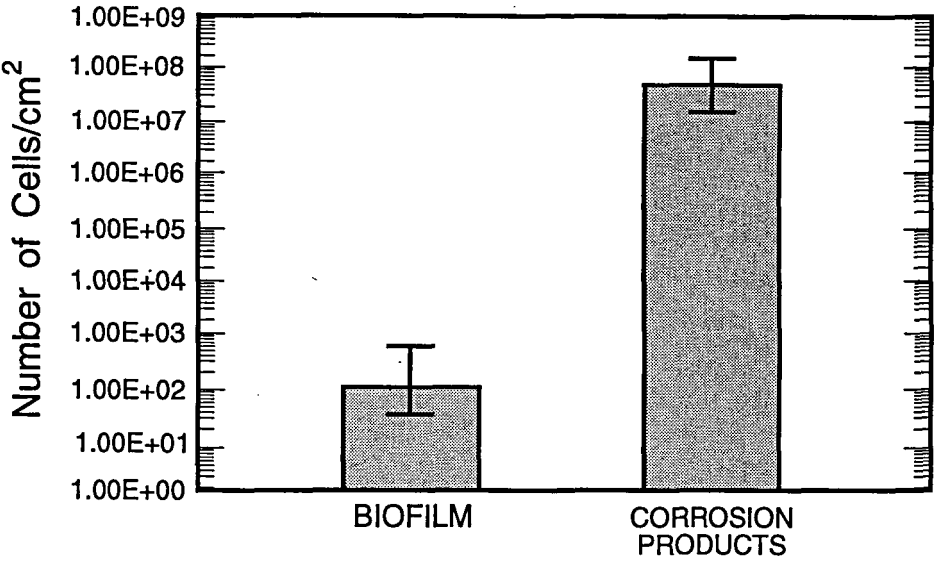

Fig. 5 Distribution of viable surfate-reducing bacteria at the uppermost part of biofilm (about 2 mm) and at the corrosion products near the metal surface (about 0.5 mm). The bars indicate 95% confidence limits.

The DC polarization measurements indicated that cathodic current decrease was accompanied with very little change in anodic current during the first 2 weeks (Fig. 7a). Both anodic and cathodic currents increased somewhat by the end of experiment (Fig. 7b). AC impedance plots indicated that only one time constant determined the corrosion

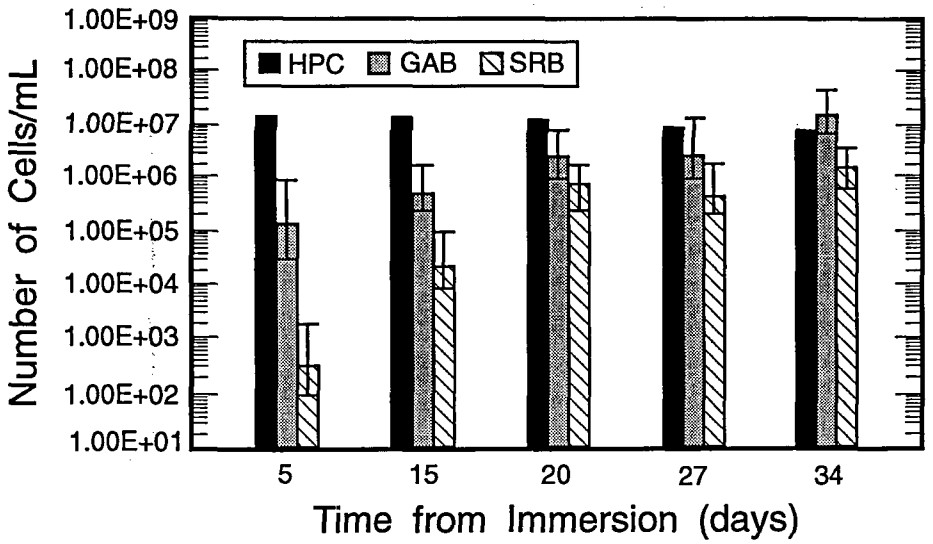

Fig. 6 Microbial accumulation in bulk liquid at different time periods. The bars indicate 95% confidence limits.

reaction at open circuit corrosion potential (Fig. 8a & b). The polarization resistance (R_p) increased rapidly from 400 ohms by the first day to 1,800 ohms by the fifth day, then again increased to 11,100 ohms by the second week. It then decreased to 4,800 ohms by the third week and to 2,500 ohms by the fifth week. Since polarization resistance is inversely proportional to the corrosion rate, results from AC impedance data indicated that the corrosion rate decreased during the first 2 weeks followed by an increase during the last 3 weeks (Fig. 9). Figure 9 also shows that surface area density of biofilm SRB increased rapidly in the second week.

The open circuit corrosion potential shifted to a more negative direction (about 80 mV) during the first week and remained constant until the end of the experiment (Fig. 10).

Surface Analysis

After biofilm and corrosion products were removed from coupons, the steel surface was black and smooth with no evidence of localized corrosion during the first 2 weeks. The AES showed that the black film consisted mainly of iron and oxygen (Fig. 11). Results from the depth profile analysis showed that the film formed on the steel surface was essentially composed of iron oxides. In the last 3 weeks, sulfur, iron, and oxygen were detected on the steel surface (Fig. 12). Bright areas were observed on the steel surface after 3 weeks (Fig. 13). These areas increased in size with time. After argon iron sputtering for 1 min (about 90 Å), the elemental map showed that the dark area was enriched with oxygen and the bright area was enriched with sulfur (Fig. 14a & b). As the sputtering penetrated deeper (1800 Å), the sulfur-rich areas were found to be underlaid with 100% iron. The dark, oxygen-rich areas were intermixed with sulfur and oxygen. At higher magnification, a high pit density was observed where a coincidence of oxygen and sulfur occurred (Figs 15a, b, & c). Sulfur was observed to be localized mostly inside the pit (d = 10 μm) as shown in Figure 15 (a) and (c), whereas oxygen was distributed in

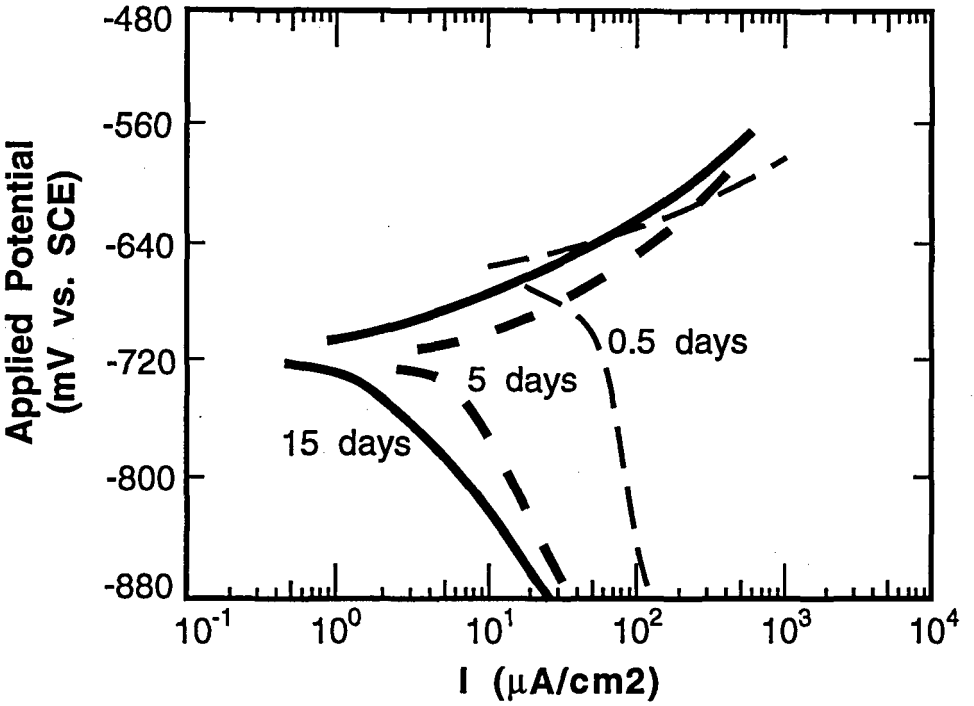

Fig. 7(a) Anodic and cathodic polarization curves within the first 2 weeks.

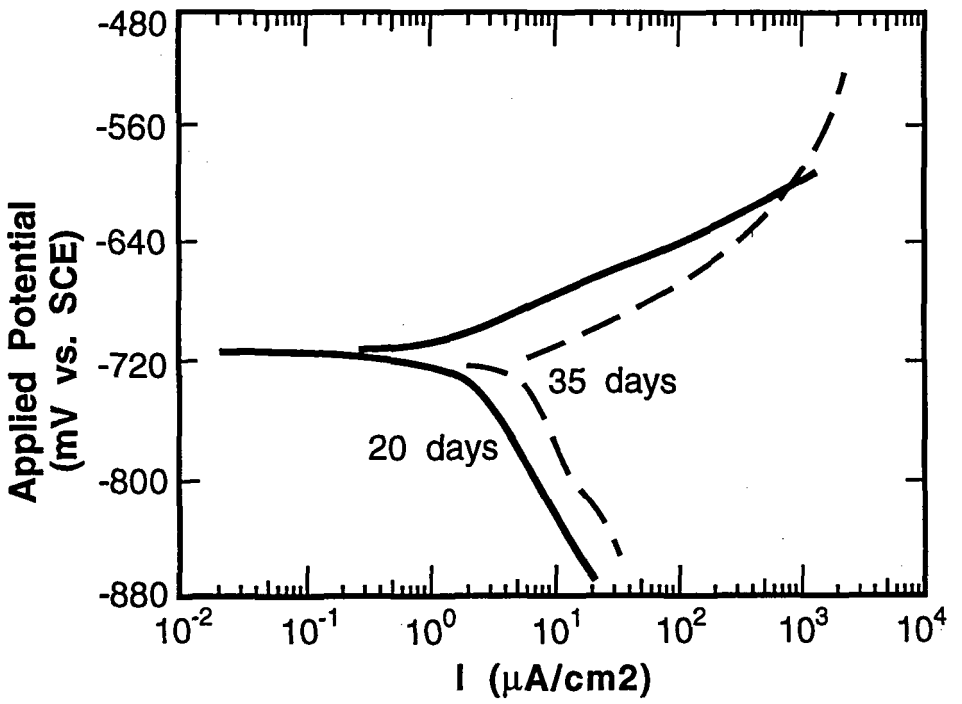

Fig. 7(b) Anodic and cathodic polarization curves within the last 3 weeks.

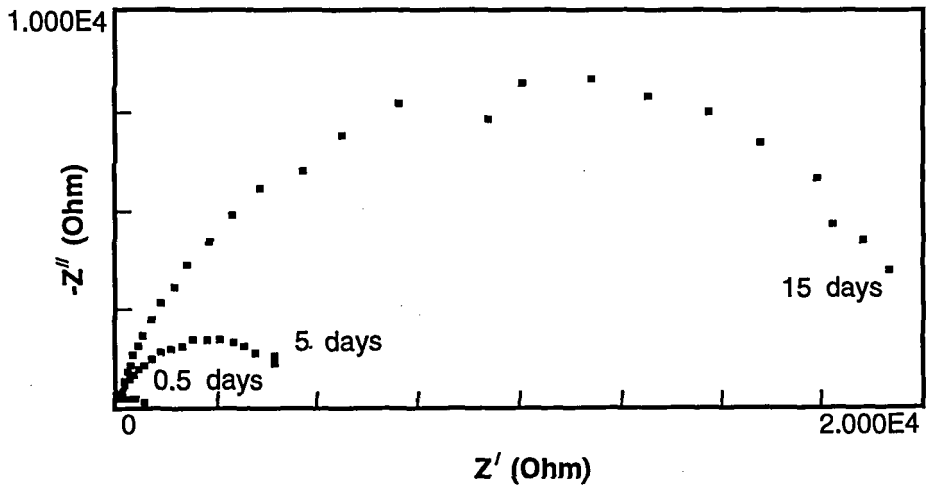

Fig. 8(a) Nyquist plots within the first 2 weeks.

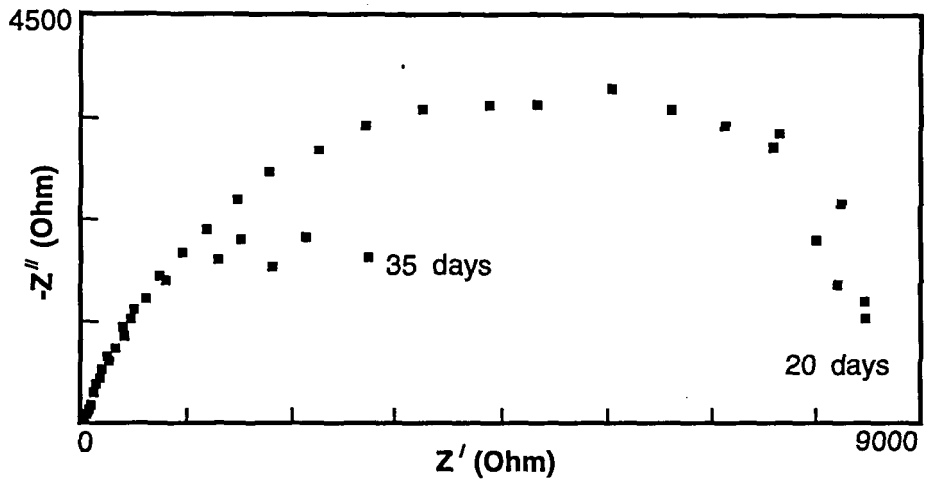

Fig. 8(b) Nyquist plots within the last 3 weeks.

the surrounding non-pitted areas as shown in Figure 15 (a) and (b). The oxygen and sulfur maps complement each other. Sputtering at 3600 Å confirmed that the bottom of the pit was enriched with sulfur (Fig. 16).

DISCUSSION

Oxygen Penetration and SRB Biofilm Development

It has been reported that in sediments SRB demonstrate maximal activity just below the aerobic/anaerobic interface (Rosser & Hamilton, 1983; Jorgensen, 1989). The present work showed that SRB proliferated in a biofilm which was totally penetrated with

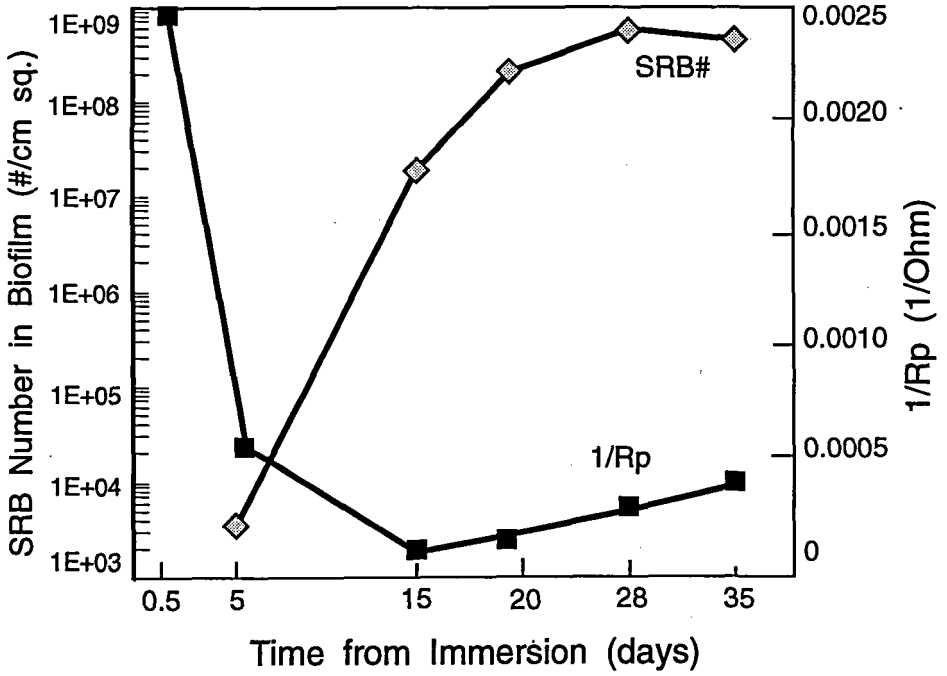

Fig. 9 Inversion of polarization resistance ($1/R_p$) and number of SRBs in biofilm at different time periods.

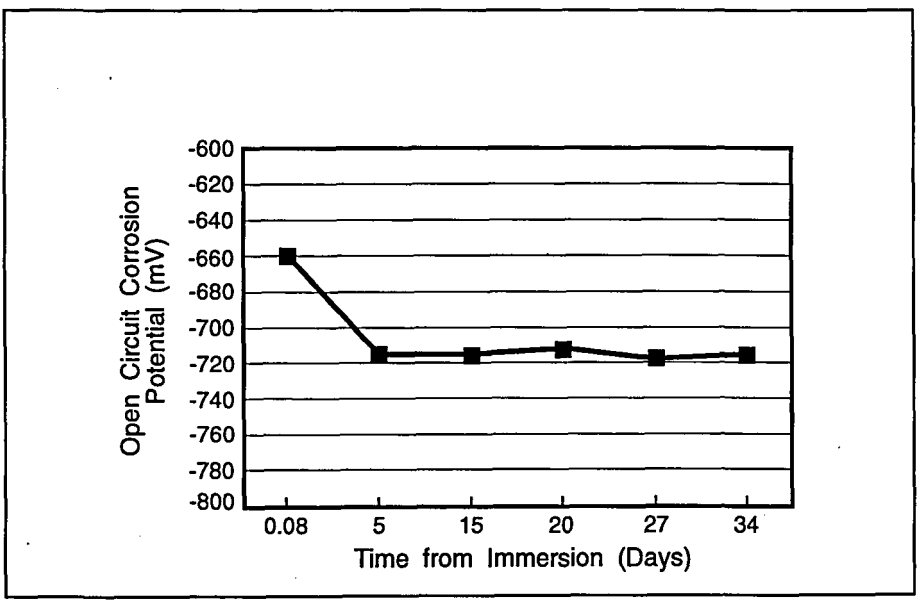

Fig. 10 Open circuit corrosion potential *vs* time.

dissolved oxygen at some locations. The biofilm was carbon-limited, and substrate consumption rates remained constant (2 g·[m^{-2}·d^{-1}]) after an initial phase of 8–10 days. Development of SRB within the aerobic biofilm was probably organic carbon limited, as demonstrated by a high concentration of sulfate (250 mg·l^{-1}) but low concentration of organic carbon (2 mg·l^{-1}) in the effluent. The highest SRB surface area density was found near the steel surface.

Oxygen consumption in the channel reactor during biofilm accumulation is attributed to: (1) microbial oxidation of organic carbon; (2) cathodic reduction by corrosion processes before an anaerobic biofilm is developed; and (3) chemical or biological oxidation of ferrous ions and reduced species (*e.g.* HS^-, FeS) after an anaerobic film is developed. Increased film thickness obstructed oxygen diffusion to the steel surface. Thus, both oxygen consumption and increased diffusional resistance provided anaerobic microniches within the biofilm for SRB growth. SRB activity was most likely restricted to microniches in a heterogeneous biofilm, as microelectrode measurements showed that a DO concentration near the steel surface ranged between 0.6 mg·l^{-1} and 1.0 mg·l^{-1} within the first 2 weeks. During the last 3 weeks, increasing deposit thickness, scavenging of oxygen by aerobic bacteria, and production of hydrogen sulfide created a reduced environment within the deposit, suitable for growth of SRB. The thickness of the anaerobic deposits was about 2000 μm by the end of the experiment (Fig. 3).

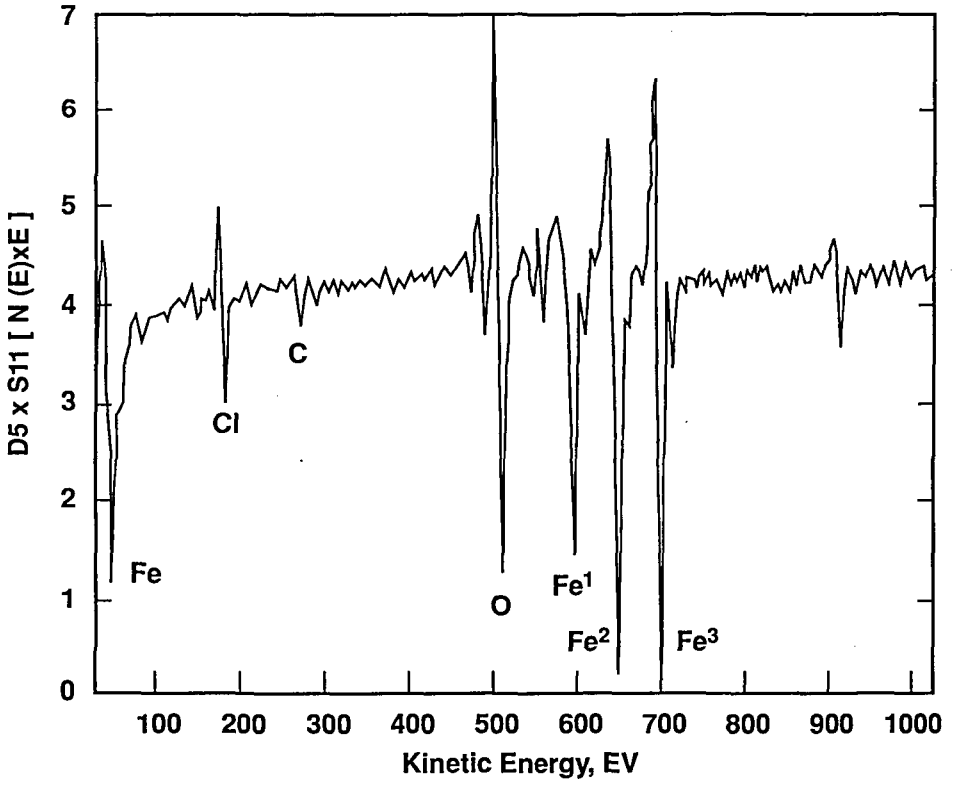

Fig. 11 Auger electron spectroscopy data for 1018 steel at the end of the second week.

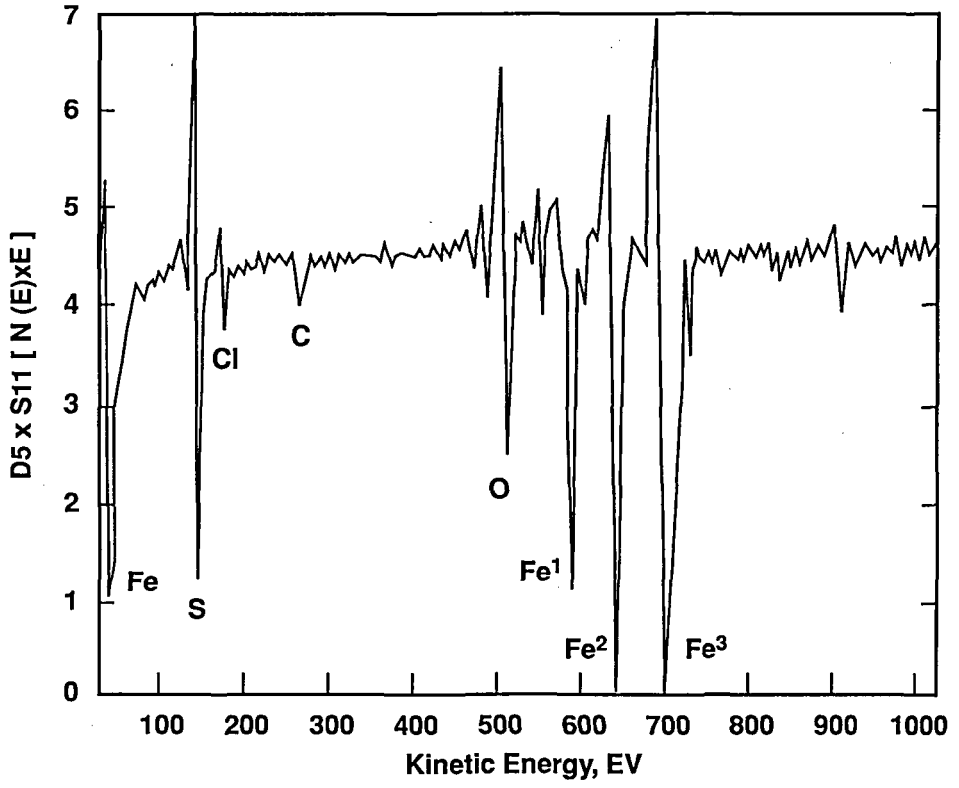

Fig. 12 Auger electron spectroscopy data for 1018 mild steel at the end of experiment

Sulfide Reaction and Transport Within the Deposits

Sulfate reduction occurred mainly near the bottom layer of the film where the SRB were present. Hydrogen sulfide may react with iron, iron oxide or oxygen, or diffuse into the bulk water. Since there was no sulfide present in the bulk liquid, it indicated that hydrogen sulfide produced by SRB was trapped within the deposits during the entire experiment. The interaction of hydrogen sulfide with dissolved oxygen or iron oxide may generate elemental sulfur, according to the following reactions (Schmitt, 1991):

$$2H_2S + O_2 \rightarrow 2H_2O + 2S^o \tag{5}$$

$$3H_2S + 2FeO(OH) \rightarrow 2FeS + 4H_2O \tag{6}$$

The number of SRB within the whole surface film increased from 3×10^4 cells·cm^{-2} at day 5 to 4×10^7 cells·cm^{-2} at day 15. Surprisingly, decreases in $1/R_p$ and cathodic current were observed during the same time. AES analysis showed no sulfur but a uniform, adherent iron oxide film at the steel surface. This indicated that the majority of hydrogen sulfide produced by SRB was consumed by oxygen or by the iron oxide precipitated around the SRB colony. An increase in $1/R_p$ and anodic and cathodic currents were observed during the final 3 weeks. AES analysis showed the presence of sulfur at the

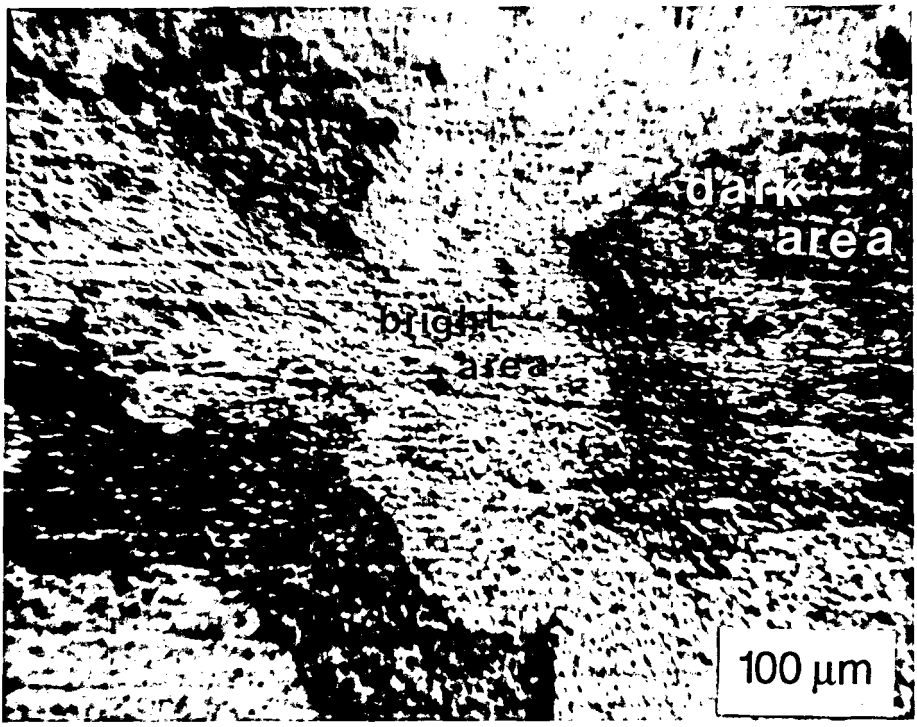

Fig. 13 Auger electron micrography of 1018 steel at the end of experiment after agar ion sputtering for 1 min (9 nm).

steel surface and that the sulfide attack was localized. The induction period of sulfide attack on steel indicated that the penetration of sulfur components (*e.g.* sulfide or sulfur) to the steel surface is the essential step for the SRB-enhanced corrosion.

It has been demonstrated (Lee & Characklis, 1993) that corrosion of mild steel was insignificant when a totally anaerobic biofilm containing SRB accumulated on the steel surface. Significant corrosion was observed, however, when the medium contained a high concentration of ferrous ions. The present results showed an initial decrease followed by an increase in corrosion rate, even when SRB proliferated during the initial stage of biofilm accumulation. Both experiments combined lead to the conclusion that environmental factors, such as oxygen and dissolved ferrous ions, as well as SRB activity, are important in determining the nature and extent of SRB-enhanced corrosion. This agrees well with suggestions by Hamilton (1991).

Corrosion Process and Mechanism

Results from AC impedance data indicated that corrosion rate decreased during the aerobic biofilm accumulation and increased after SRB developed in the biofilm. In the early stages of biofilm accumulation, the cathodic reaction was dominated by oxygen reduction, and the corrosion rate of mild steel was controlled by this process (see also Bonnel *et al.*, 1983). This was confirmed by DO profiles across the biofilm, the polarization curves, and the open circuit corrosion potential. Initial cathodic polarization

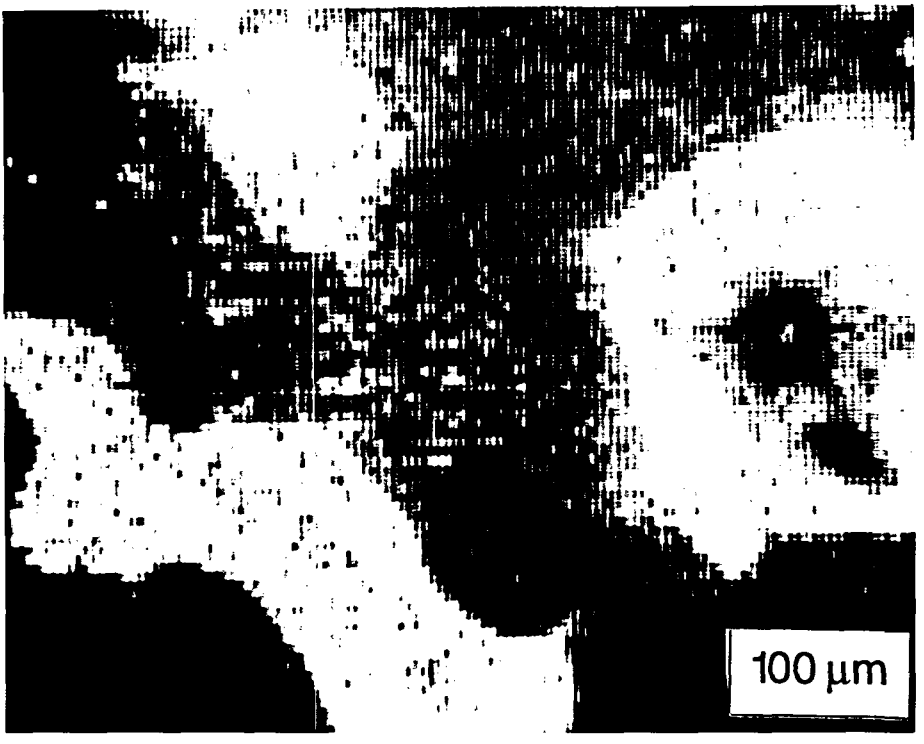

Fig. 14(a) Oxygen Auger electron map of the same area of Figure 13. The bright areas were higher in oxygen concentration relative to the dark areas.

and the reduced corrosion rate were attributed to oxygen removal by heterotrophic aerobic bacteria and limited SRB activity near the steel surface. After total depletion of oxygen near the steel surface, the cathodic depolarization and the increased corrosion rate were clearly associated with the proliferation of SRB. Cathodic depolarization may be also attributed to elemental sulfur reduction at the iron sulfide surface, as indicated by Schmitt (1991), in addition to hydrogen ion and/or hydrogen sulfide reduction:

$$S^o + H_2O + 2e^- \rightarrow HS^- + OH^- \quad (7)$$

The fact that the increased cathodic and anodic currents associated with constant open circuit corrosion potential were observed indicated that the increased corrosion rate was controlled by both anodic and cathodic reactions. The increase in corrosion rate was consistent with the observed increase of sulfide attacked areas.

CONCLUSIONS

In a biotic and aerobic biofilm system, the cathodic reaction rate of mild steel was low due to the consumption of oxygen by aerobic bacteria. As time progressed, the

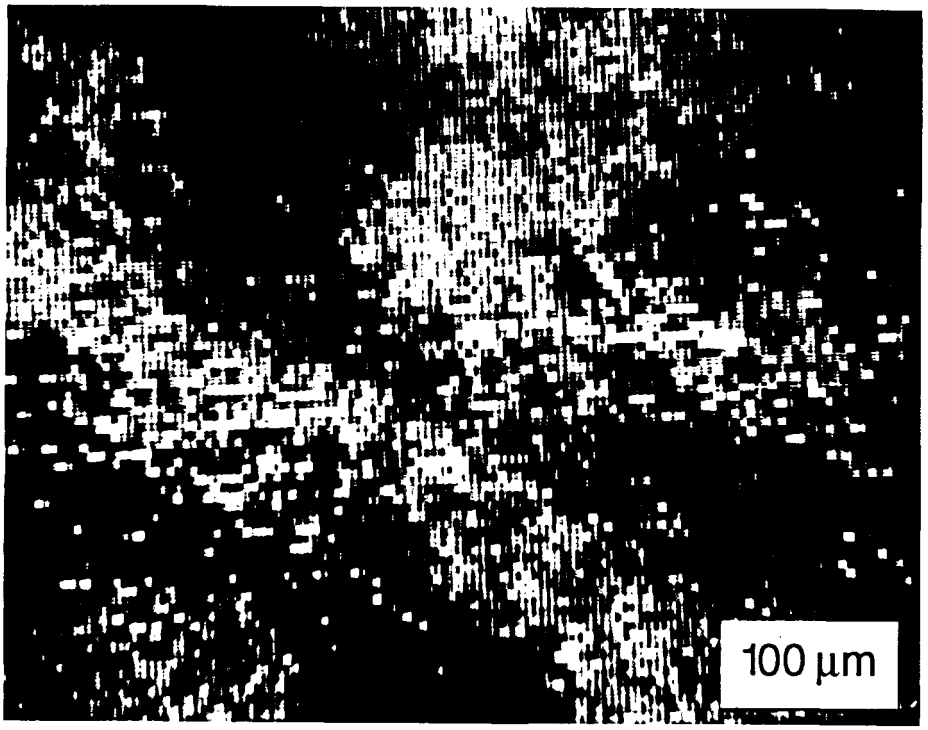

Fig. 14(b) Sulfur Auger electron map of Figure 13. The bright areas were higher in sulfur concentration relative to the dark areas.

consumption of dissolved oxygen and increasing film thickness created an anaerobic zone within the film which was suitable for SRB growth. SRB-enhanced corrosion was observed and the following conclusions were drawn:

1. The presence of SRB in an aerobic/anaerobic biofilm enhances the corrosion of mild steel through changes in both anodic and cathodic reactions.
2. Microelectrode measurements (DO and pH) are useful in determining local chemistry within the biofilm, but the local fluxes are difficult to calculate due to a filamental nature of biofilm surface.
3. AES analysis confirmed the electrochemical measurements and showed that sulfide attack is localized.

Acknowledgements

The authors express their appreciation to Dr A Hamilton and Dr P Nielsen for their helpful discussions and to Dr F Mansfield and Robert Xiao for their assistance in interpreting the AC impedance data. The authors gratefully acknowledge the cooperative agreement ECD – 8907039 between Montana State University and the National Science Foundation. The Center for Interfacial Microbial Process Engineering Industrial Associates is also acknowledged for its support of this work.

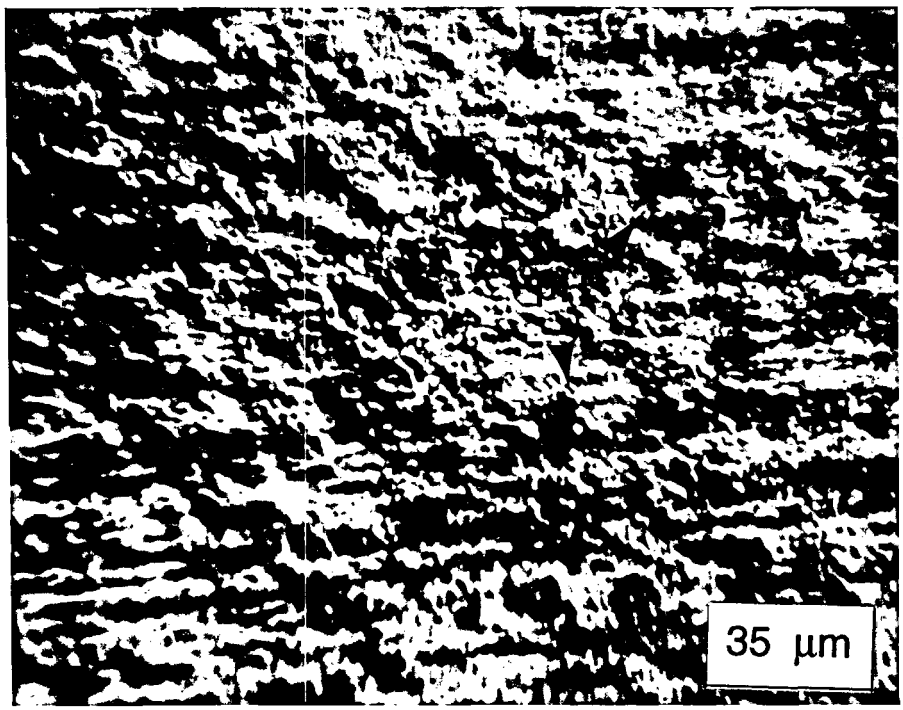

Fig. 15(a) Auger electron micrography of 1018 steel at the end of experiment after argon ion sputtering for 20 min (180 nm). A high pit density was observed where a coincidence of oxygen and sulfur occurred.

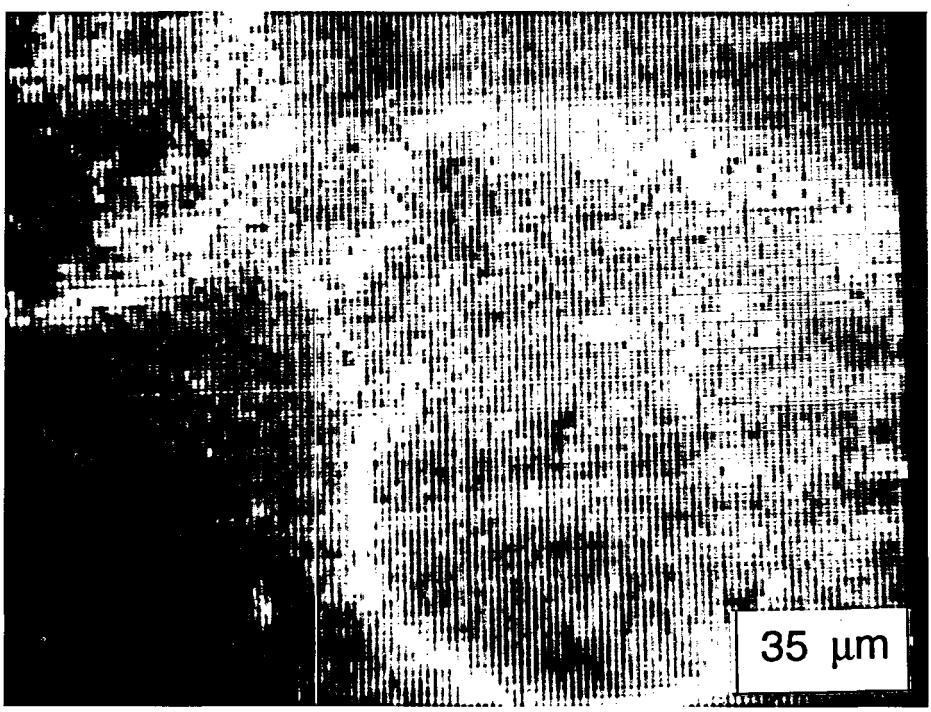

Fig. 15(b) Oxygen Auger electron map of Figure 15(a). The bright areas were higher in oxygen concentration relative to the dark areas.

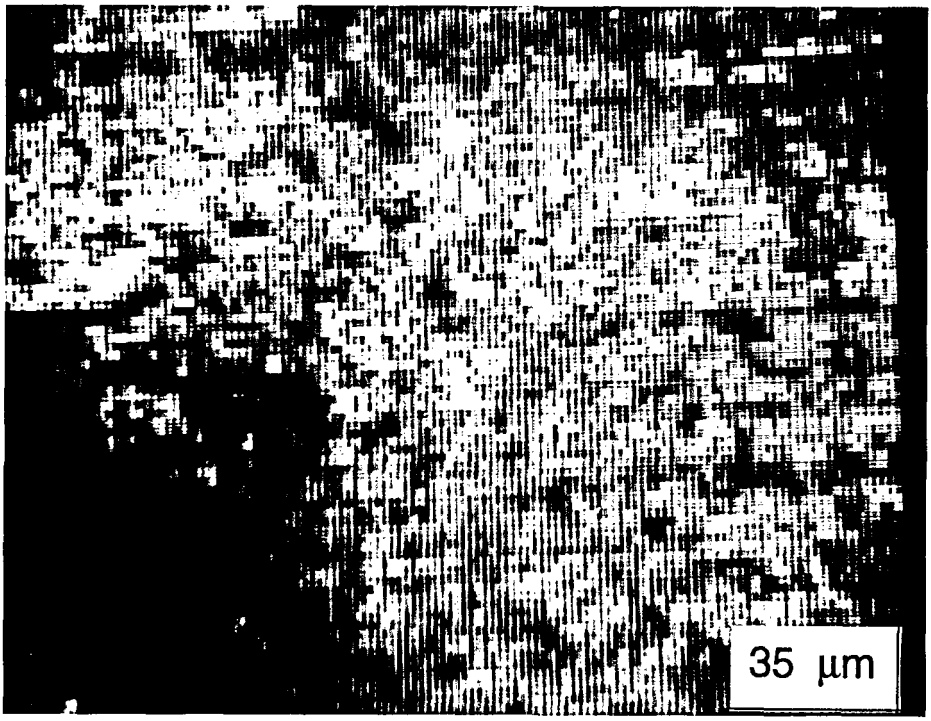

Fig. 15(c) Sulfur Auger electron map of Figure 15(a). The bright areas were higher in sulfur concentration relative to the dark areas.

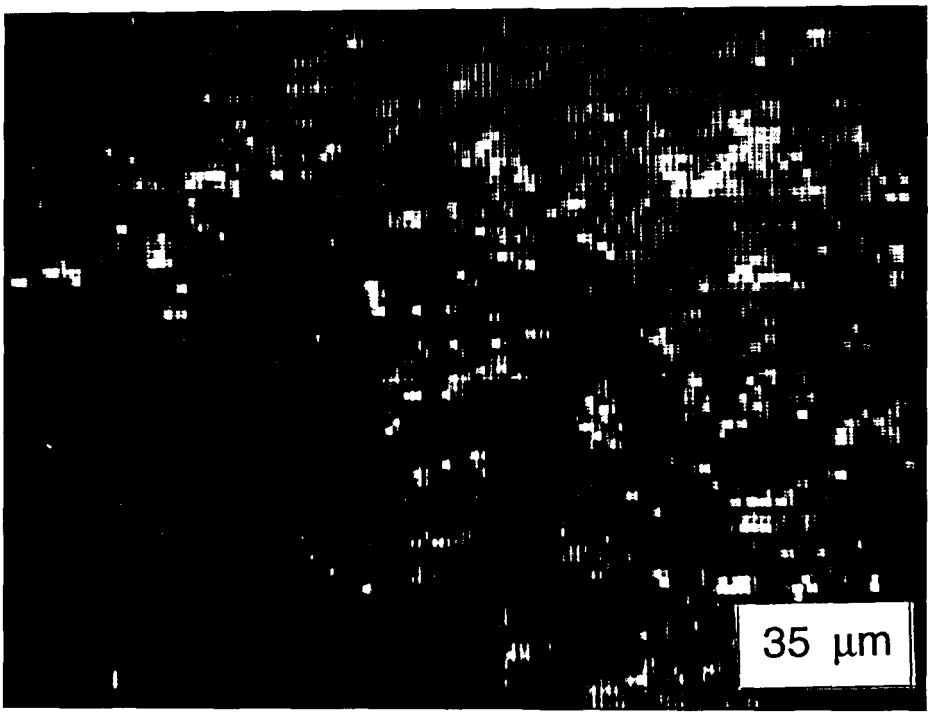

Fig. 16 Sulfur Auger electron map of the same area of Figure 15(a) after 40 mins (360 nm) argon ion sputtering. Sulfur was enriched at the bottom of the pits.

References

Bonnel A, Dabosi F, Deslouis C, Duprat M, Keddam M, Tribollet B (1983) Corrosion study of a carbon steel in natural chloride solutions by impedance techniques. *J Electrochem Soc* **130:** 753–761

Characklis W G (1990) Kinetics of microbial transformations. In: Characklis W G, Marshall K C (eds), *Biofilms*. John Wiley & Sons, New York, NY, pp 233–264

Clesceri L S, Greenberg A E, Trussell R R (eds) (1989) *Standard Methods for the Examination of Water and Wastewater* (17 edn). APHA-AWWA-WPCF, Washington, DC pp 9–77–9–80

Costello J A (1974) Cathodic depolarization by sulfate-reducing bacteria. *S Afr J Sci* **70:** 202–204

Emmanual J and Hornbeck C (1987) A rapid embedding method for large undeclacified bone and implant in PMMA. *Stain Technol* **62:** 401–410

Hamilton W A (1990) Sulfate-reducing bacteria and their role in microbially influenced corrosion. In: *Proc Int Symp Microbially Influenced Corrosion. Knoxville*, TN, pp i–iv

Hamilton W A (1991) Sulfate-reducing bacteria and their role in biocorrosion. In: Fleming H C, Geesey G (eds) *Biofouling and Biocorrosion in Industrial Water Systems*. Springer-Verlag, Berlin, pp 187–193

Hamilton W A, Maxwell S (1985) Biological and corrosion activities of sulfate-reducing bacteria within natural biofilms. In: Dexter S C (ed) *Proc Int Conf Biologically Induced Corrosion*. National Association of Corrosion Engineers, Houston, Texas, pp 131–136

Hardy J A, Brown J L (1984) The corrosion of mild steel by biogenic sulfide film exposed to air. *Corrosion* **40:** 650–654

Jorgensen B B (1989) Biochemistry of chemoautotrophic bacteria. In: Schlegel H G, Bowien B (eds) *Autotrophic Bacteria*. Science Techn Publ pp 117–146

Kending M W, Meyer E, Lindberg G, Mansfeld F (1983) CIRFIT, a computer analysis of electrochemical impedance data. *Corrosion Sci* **23:** 1007–1015

King R A, Miller J D A, Smith J S (1973) Corrosion of mild steel by iron sulfides. *Br Corros J* **8:** 137–141

Lee W, Characklis W G (1993) Corrosion of mild steel under an anaerobic biofilm. *Corrosions* (in press)

Lewandowski Z, Lee W, Characklis W G, Little B J (1989) Dissolved oxygen and pH microelectrode measurements at water immersed metal surface. *Corrosion* **45:** 92–97

Moosavi A N, Pirrie R S, Hamilton W A (1990) Effect of sulfate-reducing bacteria activity on performance of sacrificial anodes. In: *Proc Int Symp Microbially Influenced Corrosion*. Knoxville, TN, pp 3–13

Rosser H R, Hamilton W A (1983) Simple assay for accurate determination of [35S] sulfate reduction activity. *Appl Environ Microbiol* **45:** 1956–1959

Schmitt G (1991) Effect of elemental sulfur on corrosion in sour gas systems. *Corrosion* **47:** 285–308

Smith J S, Miller J D A (1975) Nature of sulfides and their corrosive effect on ferrous metals: a review. *Br Corros J* **10:** 136–143

Starkey R L (1985) Anaerobic corrosion – perspectives about causes. In: Dexter S C (ed) *Proc Int Conf Biologically Induced Corrosion*. National Association of Corrosion Engineers, Houston, TX, pp 3–7

VanHoudt P, Lewandowski Z, Little B J (1992) Construction and application of an iridium oxide microelectrode. *Biotechnol Bioeng*, (in press)